

Computational modeling of laser-induced self-organization in nanoscopic metal films for predictive nanomanufacturing

Justin Trice^{a,b}, Ramki Kalyanaraman^{a,b}, Radhakrishna Sureshkumar,^{b,c}

^aDepartment of Physics, Washington University, St. Louis, Missouri 63130, USA;

^bCenter for Materials Innovation, Washington University, St. Louis, Missouri 63130, USA;

^cDepartment of Energy, Environmental and Chemical Engineering, Washington University, St. Louis, Missouri 63130, USA

ABSTRACT

Computer models that accurately predict the dynamics of nanoscale self-organization are vital towards knowledge-based nanomanufacturing. Here we present a first principles computational model of laser induced self-organization of thin metallic films (thickness ≤ 30 nm) into nanoscale patterns which eventually evolve into ordered nanoparticles. The pattern formation is initiated by a thin film hydrodynamic instability and the ensuing length scales are related to the intrinsic materials properties such as surface tension and van der Waals' dispersion forces. We discuss a fully implicit, finite-difference method with adaptive time step and mesh size control for the solution of the nonlinear, fourth-order PDE governing the thin film dynamics. These simulations capture the changing morphology of the film due to the competition between surface tension and van der Waals forces. Simulation results are used to understand the nonlinear amplification of film height perturbations $\sim (KT/\gamma)^{1/2}$, where K , T and γ represent the Boltzmann constant, absolute temperature, and surface tension respectively, leading eventually to film rupture.

Keywords: thin film, process modeling, nanoparticles, lubrication equation, finite-difference

1. INTRODUCTION

Mode-predictive nanomanufacturing will play a central role in the design and fabrication of the next generation of devices for information processing, photonic, and electronic applications. First principles computational models allow for rapid differentiation between different designs and process optimization. A promising avenue for the fabrication of novel nanoscopic devices is self-organization of nanoparticles via dewetting of thermodynamically unstable, metallic thin films. Thin-film systems with thicknesses ~ 100 nm deposited on a substrate, such as SiO_2 , are thermodynamically unstable due to the competition between long-range intermolecular interactions and stabilizing surface tension forces.¹⁻³ Pulsed laser irradiation of such systems fosters this instability giving rise to nano-scale features with a characteristic length scale that may be tuned by varying the processing parameters.^{4,5} While both linear and nonlinear analysis can predict the characteristic length scale for such systems,⁶ the nonlinear self-organization pathway is typically characterized by a "tipping point" at which the dynamics become ultrafast. The inability of linearized models to capture such inherently nonlinear physics and the need to map out the dynamics landscape of self-organization motivate fully nonlinear analysis of such systems. Here, we present an efficient and accurate algorithm for solving the thin-film equation that governs the dewetting dynamics. Code validation and results for isothermal dewetting dynamics are presented.

Further author information: (Send correspondence to R.S.)

J.T.: E-mail: jtrice@physics.wustl.edu

R.K.: E-mail: ramkik@wuphys.wustl.edu

R.S.: E-mail: suresh@che.wustl.edu

2. ALGORITHM

For the system of interest, the characteristic length scale that emerges from spontaneous rupture of thin films ≤ 30 nm is much greater than molecular scales.² Therefore, continuum-level modeling may be used to describe the dewetting dynamics. Thus, we have employed the thin-film hydrodynamic (TFH) equation used by Vrij^{2,3} and Sharma and Ruckenstein⁷ in this study:

$$3\mu \frac{\partial h}{\partial t} + \nabla \cdot (\gamma h^3 \nabla \nabla^2 h + \frac{A^*}{h} \nabla h) = 0 \quad (1)$$

where μ represents the viscosity of the fluid, $h = h(\mathbf{x}, t)$ is the film's height, γ is the surface tension of the film, and $A^* \equiv \frac{A}{2\pi}$ where A is the Hamaker coefficient representing the strength of the effective pressure gradient arising from long-range intermolecular forces due to van der Waals interactions. For the case of liquid Co just at the melting temperature, $\mu = 4.46 \times 10^{-3}$ Pa-s, $\gamma = 1.88$ J-m⁻², and the typical range of Hamaker coefficient for metals is $10^{-20} \leq A \leq 10^{-18}$ J.⁴ For the purposes of the present study, we consider the case of height variation with respect to space exclusively in the x -direction (i.e. system is treated as a 1D film). Thus, Eq. 1 reduces to

$$3\mu \frac{\partial h}{\partial t} + \frac{\partial}{\partial x} (\gamma h^3 \frac{\partial^3 h}{\partial x^3} + \frac{A^*}{h} \frac{\partial h}{\partial x}) = 0 \quad (2)$$

Numerical discretization is based on the finite-difference technique outline in Ref.⁸ Specifically, Eq. 2 is discretized as follows

$$3\mu(h_k^{n+1} - h_k^n) + \Delta t^n (f_k^{n+1} + g_k^{n+1}) = 0 \quad (3)$$

where

$$f_k^{n+1} = \frac{D_{k-1} h_{k-2}^{n+1}}{\Delta x^4} - \frac{(3D_{k-1} + D_k) h_{k-1}^{n+1}}{\Delta x^4} - \frac{(D_{k-1} + 3D_k) h_{k+1}^{n+1}}{\Delta x^4} + \frac{D_k h_{k+2}^{n+1}}{\Delta x^4} + \frac{(3D_{k-1} + 3D_k) h_k^{n+1}}{\Delta x^4} \quad (4)$$

and

$$g_k^{n+1} = \frac{G_{k-1} h_{k-1}^{n+1}}{\Delta x^2} + \frac{G_k h_{k+1}^{n+1}}{\Delta x^2} - \frac{(G_{k-1} + G_k) h_k^{n+1}}{\Delta x^2} \quad (5)$$

with discretized diffusion and Hamaker terms expressed by

$$D_k = \frac{2\gamma(h_{k+1}^{n+1} h_k^{n+1})^2}{h_{k+1}^{n+1} + h_k^{n+1}} \quad (6)$$

and

$$G_k = \frac{A^*}{2} \left(\frac{1}{h_k^{n+1}} + \frac{1}{h_{k+1}^{n+1}} \right) \quad (7)$$

where Δt^n and Δx correspond to the current timestep and spacing between the nodes respectively. In Eqs. 3 to 7, the super- and sub-scripts denote discretized time steps and the node location. The highest order term in the equation has a pronounced influence on the nonlinear dynamics. Thus, care must be taken when discretizing the diffusion coefficient (Eq. 6). This approach preserves positivity ($h_k^{n+1} > 0 \forall n$) so that negative values of film thickness are not reported – especially problematic when $h \rightarrow 0$.⁸⁻¹⁰ Periodic boundary conditions are imposed on the spacial domain. Typically, the domain size R is chosen to be a few integer multiples of the wavelength of the fastest growing mode expected from linear stability analysis (LSA). At the domain ends the boundary conditions

$$h(t, x) |_{x=0} = h(t, x) |_{x=R} \quad (8)$$

and

$$\frac{\partial h(t, x)}{\partial x} \Big|_{x=0} = \frac{\partial h(t, x)}{\partial x} \Big|_{x=R} \quad (9)$$

are imposed. The analogous discretized expressions are as follows (where N is the number of nodes in the spatial domain)

$$h_{N-2}^{n+1} = h_3^{n+1} \quad (10)$$

and

$$h_4^{n+1} = h_{N-1}^{n+1} \quad h_{N-3}^{n+1} = h_2^{n+1} \quad h_{N-4}^{n+1} = h_1^{n+1} \quad h_N^{n+1} = h_5^{n+1} \quad (11)$$

The system of nonlinear equations that arise from the numerical discretization was solved using the Newton-Raphson method. Namely, the solution at t^{n+1} is obtained iteratively by starting from a guess value h_k^* as

$$h_k^{n+1} = h_k^* + \delta h_k \quad (12)$$

where δh_k is the correction to the initial guess. The residual R_k at each node is written as

$$R_k = -3\mu(h_k^* - h_k^n) - \Delta t^n (f_k^* + g_k^*) \quad (13)$$

where f_k^* and g_k^* are given by Eqs. 4 and 5 by replacing h_k^{n+1} with h_k^* . Thus, to determine δh_k , one solves the system of linear equations given by

$$\mathbf{J}_{k,1} \delta h_k = R_k \quad (14)$$

with $\mathbf{J}_{k,1} = \frac{\delta R_k}{\delta h_k}$ being the Jacobian matrix. Note that for the problem discussed here, the Jacobian matrix consists of N rows with at most 5 non-zero elements in each. The initial guess for the solution is taken to be $h_k^* = h_k^n$. If at any value of k Eq. 13 exceeds a certain tolerance (here a tolerance of between $10^{-10} - 10^{-8}$ nm is used), then $h_k^* + \delta h_k$ is taken as the new guess and the iteration is repeated until convergence is obtained.

To ensure that the algorithm converges in a reasonable number of iterations, an optimum value of the time step is determined dynamically (as described in Ref.⁸). The relative error E_k of the numerical solution at any point k is given by

$$E_k = \frac{2\Delta t^n}{\Delta t^{n-1}} \frac{\Delta t^{n-1} h_k^{n+1} + \Delta t^n h_k^{n-1} - (\Delta t^{n-1} + \Delta t^n) h_k^n}{(\Delta t^{n-1} + \Delta t^n) h_k^n}. \quad (15)$$

If E_k is less than some tolerance for all values of k (a tolerance value between of $10^{-10} - 10^{-8}$ ns was chosen), then the solution h_k^{n+1} obtained using time step Δt^n is accepted. If not, then the time step is decreased (namely, $\Delta t^n \rightarrow \frac{1}{2} \Delta t^n$) and the spatial domain solution is resolved (i.e. Eq. 14 is solved until convergence is reached with the new time step value). Once convergence with respect to both space and time is obtained, the next guess for the time step is taken to be $\Delta t^n = 2\Delta t^{n-1}$ and the entire process is repeated.

3. CODE VALIDATION AND RESULTS

In order to validate the code, we first compare the growth rate predicted by the linear stability theory to the initial rate of growth of sinusoidal perturbations since nonlinear effects are not apparent during early stages of nonlinear simulation. First, one considers the linearized form of Eq. 1 by assuming infinitesimally small perturbations h' that are imposed on an initially flat film of initial thickness h_o (i.e. let $h \rightarrow h_o + h'$) and keeping only terms linear in h' . Thus, Eq. 1 becomes

$$3\mu \frac{\partial h'}{\partial t} + \nabla \cdot (\gamma h_o^3 \nabla \nabla^2 h') + \frac{A^*}{h_o} \nabla h' = 0. \quad (16)$$

Next, we substitute the normal mode form for 1-dimension, namely $h' = \epsilon \exp(ikx + \sigma t)$ where σ denotes the growth/decay of perturbations with wavenumber k . This yields the dispersion relation:

$$3\mu\sigma = -\gamma h_o^3 k^4 + \frac{A^*}{h_o} k^2. \quad (17)$$

From Eq. 17 the fastest growing mode (k_{max}) can be obtained by letting $\frac{\partial \sigma}{\partial k} = 0$ and the corresponding wavelength $\Lambda \equiv 2\pi/k_{max}$ is given by:

$$\Lambda = \sqrt{\frac{16\pi^3\gamma}{A}} h_0^2. \quad (18)$$

Further, a characteristic time scale $\tau_d = 2\pi/\sigma_{max}$ may be defined by substituting k_{max} back into Eq. 17. Explicitly, τ_d is given by

$$\tau_d = \frac{96\pi^3\gamma\mu h_0^5}{A^2}. \quad (19)$$

For comparison, the nonlinear code was initialized with a sinusoidal perturbation $h(t, x)|_{t=0} = \nu \sin(\frac{2\pi}{L}x)$ with $\nu = 0.01$ nm. The domain size R was taken to be equal to 2Λ . Simulations were performed for L values of 2Λ , 1.5Λ , Λ , and 0.75Λ . The growth rates for the various simulations were determined by considering the normal mode form of the height evolution at the node representing the maximum of the sinusoidal perturbation (i.e. evolution at the node x_{max} at which h takes its max value is given by $h(t, x)|_{x=x_{max}} = h(0, x)|_{x=x_{max}} \exp(\sigma t) + h(0, x)|_{x=x_{max}}$). The value of $\ln((h(t, x)|_{x=x_0} - h(0, x)|_{x=x_0})/h(0, x)|_{x=x_0})$ versus t was plotted and σ was determined by taking the slope of this line. Fig. 1 presents a typical calculation of the growth rate. For the case of a 10 nm thick Co film on SiO₂ using Hamaker coefficient value of $A^* = 10^{-18} J$. A value of $\sigma = 9.988 \times 10^4$ s⁻¹ was determined from the nonlinear simulation which is in good agreement to the LSA-predicted value of $\sigma = 9.938 \times 10^4$ s⁻¹. Fig. 2 shows that the excellent agreement between the dispersion relationship predicted by LSA and the growth rates obtained from nonlinear simulations.

In addition, the algorithm was found to be robust with respect to initial conditions and domain size. The result of simulating the dewetting evolution of a 1 nm Co thin film on SiO₂ with an initial perturbation expressed as $\nu \sin(\frac{\pi}{\Lambda}x)$, the period being equal to twice that of the characteristic wavelength, is presented in Fig.3. Simulations were conducted for domain sizes given by $R = 2\Lambda$, 6Λ , and 12Λ . The result was independent of the domain size used. In addition, Figs. 3(d-e) present the Fast-Fourier transforms (FFT) of the film height $h(x, t)$ at $t = 0.00$ ns and $t = 1.00$ ns. Transfer of energy from the mode denoting 2Λ to smaller modes is evident with the largest contribution going to the characteristic mode Λ . The growth of the Λ mode with other modes still persisting in the dynamics gives rise to a distinct “twinning” feature at the peaks in the periodic solution (i.e. the splitting of the height profile).

To further probe the effects of initial conditions on dewetting evolution, the nonlinear Co-SiO₂ thin film model was initialized via random perturbations. An initial film thickness of 10 nm was perturbed via random perturbations sampled from a uniform distribution (mean value zero; variance = $\frac{1}{3} \frac{KT_{melt}}{\gamma_{ave}}$) with a maximum/minimum amplitude given by $\pm \sqrt{\frac{KT_{melt}}{\gamma_{ave}}}$ where K is the Boltzmann constant and $T_{melt} = 1768$ K corresponds to the Co film’s melting temperature. The initial state of the film and subsequent evolution are shown in Fig. 4(a-c). From Fig. 4(d), note that interfacial dynamics proceed rather slowly until a critical “tipping” point at which the intermolecular terms become dominant. Then, the ensuing dynamics become ultrafast. For the case of 10 nm of Co with a Hamaker value of $A^* = 10^{-18}$ J, this critical point is near $55.5 \mu s$ leading up to film rupture at $62.5 \mu s$.

4. CONCLUSIONS

In summary, we have developed and validated an algorithm to solve the highly nonlinear fourth-order PDE governing thin film hydrodynamics. Excellent agreement between the predictions was found for the initial growth rates of sinusoidal perturbations and those obtained from LSA. The algorithm is robust against various initial conditions including sinusoidal perturbations of varying periods and random perturbations. In addition, the periodic solution is not affected by the domain size. The algorithm can be readily extended to 2-dimensional systems. Further, non-isothermal processing conditions can also be addressed by suitably modifying the code to incorporate thermal transport. These extensions are currently under investigation.

ACKNOWLEDGMENTS

R.K. and R.S. acknowledge support by the National Science Foundation through CAREER Grant No. DMI-0449258 and No. CTS-0335348, respectively.

REFERENCES

1. A. Sharma, "Relationship of thin film stability and morphology to macroscopic parameters of wetting in the apolar and polar systems," *Langmuir* **9**, pp. 861–869, 1993.
2. A. Vrij, "Possible mechanism for the spontaneous rupture of thin, free liquid films," *Discussions of the Faraday Society* **42**, pp. 23–27, 1966.
3. A. Vrij and J. Overbeek, "Rupture of thin liquid films due to spontaneous fluctuations in thickness," *Journal of the American Chemical Society* **90**, pp. 3074–3078, 5 June 1968.
4. C. Favazza, R. Kalyanaraman, and R. Sureshkumar, "Robust nanopatterning by laser-induced dewetting of metal nanofilms," *Nanotechnology* **17**, pp. 4229–4234, 2006.
5. J. Trice, D. Thomas, C. Favazza, R. Sureshkumar, and R. Kalyanaraman, "Pulsed-laser-induced dewetting in nanoscopic metal films: Theory and experiments," *Physical Review B* **75**, p. 235439, 2007.
6. A. Sharma and K. Rajesh, "Pattern Formation in Unstable Thin Liquid Films," *Physical Review Letters* **81**(16), pp. 3463–3466, 1998.
7. A. Sharma and E. Ruckenstein, "Finite-amplitude instability of thin free and wetting films: prediction of lifetimes," *Langmuir* **2**, pp. 480–94, 1986.
8. J. Diez and L. Kondic, "Computing Three-Dimensional Thin Film Flows Including Contact Lines," *Journal of Computational Physics* **183**, pp. 274–306, 2002.
9. L. Kondic, "Instabilities in gravity driven flow of thin fluid films," *SIAM Review* **45**(1), pp. 95–115, 2003.
10. L. Zhornitskaya and A. Bertozzi, "Positivity-Preserving Numerical Schemes for Lubrication-Type Equations," *SIAM Journal of Numerical Analysis*. **37**(2), pp. 523–555, 2000.

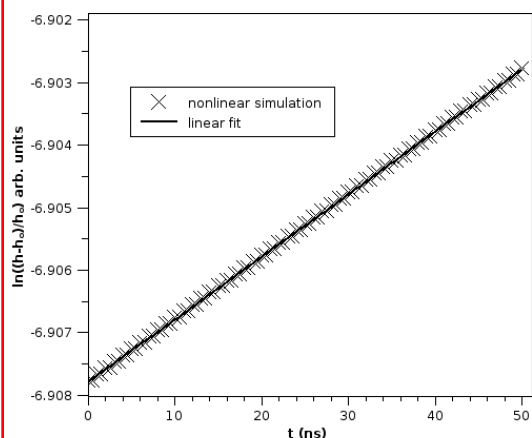


Figure 1. Typical calculation of growth rate σ at the initial stage of the nonlinear simulation for the case of 10 nm of Co on SiO₂ using $A^* = 10^{-18} J$. The initial perturbation was of the form $h(x, t)|_{t=0} = \nu \sin(\frac{2\pi}{T}x)$ and possessed a period equal to the characteristic wavelength $T = \Lambda$. A value of $\sigma = 9.988 \times 10^4 \text{ s}^{-1}$ was determined for the nonlinear simulation compared to value of $\sigma = 9.938 \times 10^4 \text{ s}^{-1}$ predicted by linear stability analysis.

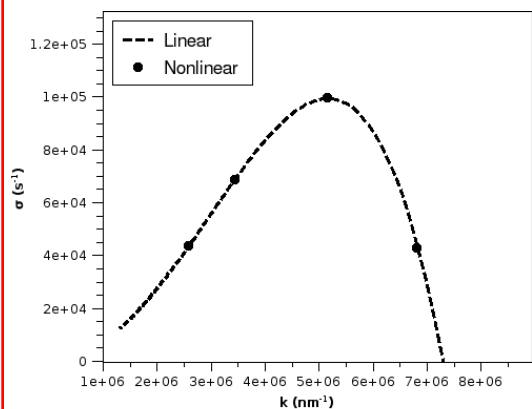


Figure 2. Comparison of growth rates σ at early stage of the nonlinear simulation with the LSA prediction for the case of 10 nm of Co on SiO₂ using $A^* = 10^{-18} J$. Nonlinear simulations were performed on a domain size $R = 2\Lambda$. The nonlinear model was initialized with sinusoidal perturbation on the form $h(t, x)|_{t=0} = \nu \sin(\frac{2\pi}{T}x)$ with $\nu = 0.01$ and simulations performed for the cases $T = 2\Lambda, 1.5\Lambda, \Lambda$, and 0.75Λ .

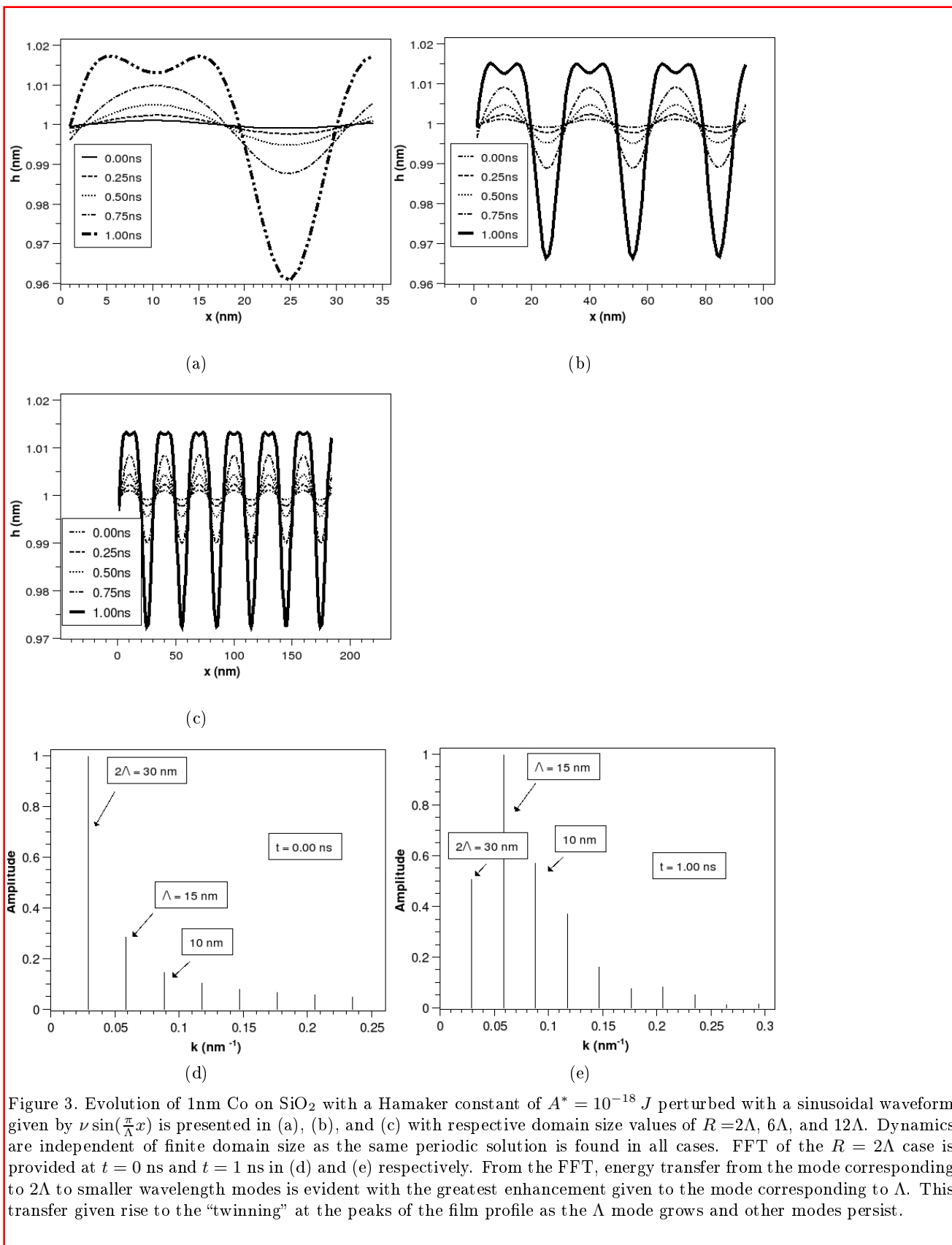


Figure 3. Evolution of 1nm Co on SiO₂ with a Hamaker constant of $A^* = 10^{-18} J$ perturbed with a sinusoidal waveform given by $\nu \sin(\frac{\pi}{\Lambda}x)$ is presented in (a), (b), and (c) with respective domain size values of $R = 2\Lambda$, 6Λ , and 12Λ . Dynamics are independent of finite domain size as the same periodic solution is found in all cases. FFT of the $R = 2\Lambda$ case is provided at $t = 0$ ns and $t = 1$ ns in (d) and (e) respectively. From the FFT, energy transfer from the mode corresponding to 2Λ to smaller wavelength modes is evident with the greatest enhancement given to the mode corresponding to Λ . This transfer given rise to the “twinning” at the peaks of the film profile as the Λ mode grows and other modes persist.

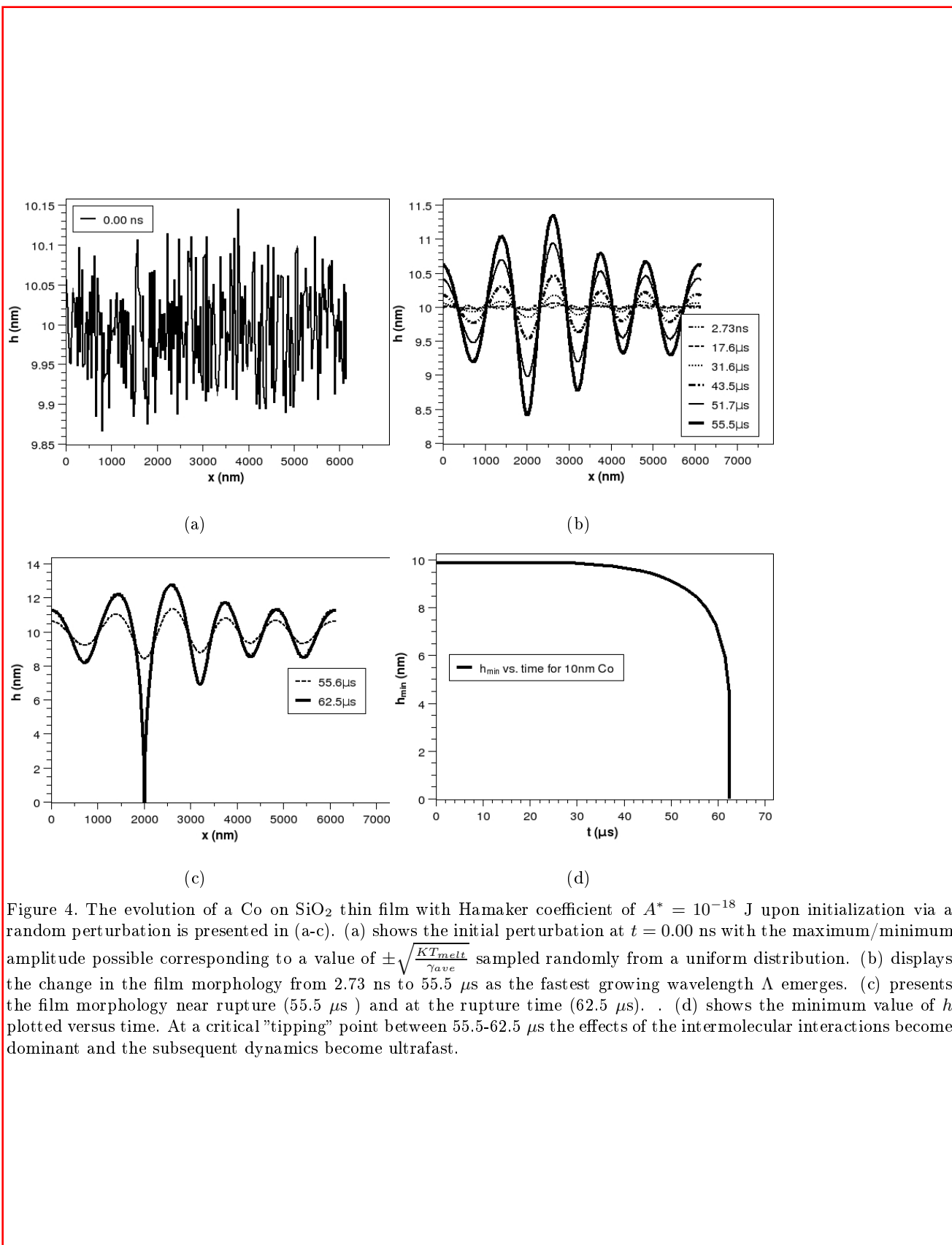


Figure 4. The evolution of a Co on SiO₂ thin film with Hamaker coefficient of $A^* = 10^{-18}$ J upon initialization via a random perturbation is presented in (a-c). (a) shows the initial perturbation at $t = 0.00$ ns with the maximum/minimum amplitude possible corresponding to a value of $\pm \sqrt{\frac{KT_{melt}}{\gamma_{ave}}}$ sampled randomly from a uniform distribution. (b) displays the change in the film morphology from 2.73 ns to 55.5 μ s as the fastest growing wavelength Λ emerges. (c) presents the film morphology near rupture (55.5 μ s) and at the rupture time (62.5 μ s). (d) shows the minimum value of h plotted versus time. At a critical "tipping" point between 55.5 - 62.5 μ s the effects of the intermolecular interactions become dominant and the subsequent dynamics become ultrafast.